Fluid Phase Equilibria 544–545 (2021) 113094

Contents lists available at ScienceDirect

Fluid Phase Equilibria

journal homepage: www.elsevier.com/locate/fluid

Application of deep neural network (DNN) for experimental liquid-liquid equilibrium data of water + butyric acid + 5-methyl-2-hexanone ternary systems

Sezin Bekri[a], Dilek Özmen[a], Aykut Türkmenoğlu[b], Atilla Özmen[c,*]

[a] Dept. of Chemical Engineering, Istanbul University-Cerrahpaşa, Istanbul, Turkey
[b] Directorate of Food Control Laboratory, Republic of Turkey Ministry of Food Agriculture and Livestock Tekirdağ, Turkey
[c] Dept. of Electrical–Electronics Engineering, Kadir Has University, Istanbul, Turkey

ARTICLE INFO

Article history:
Received 9 January 2021
Revised 1 May 2021
Accepted 17 May 2021
Available online 20 June 2021

Keywords:
Liquid-liquid equilibrium (LLE)
Deep neural network (DNN)
Butyric acid
5-Methyl-2-hexanone
Thermodynamic models

ABSTRACT

LLE data are important for simulation and design of extraction equipment. In this study, deep neural network (DNN) structure was proposed for modelling of the ternary liquid-liquid equilibrium (LLE). LLE data of (water + butyric acid + 5-methyl-2-hexanone) ternaries defined at three different temperatures of 298.2, 308.2, and 318.2 K and P = 101.3 kPa, were obtained experimentally and then correlated with nonrandom two-liquid (NRTL) and universal quasi-chemical (UNIQUAC) models. The performance of the proposed DNN model was compared with that of NRTL and UNIQUAC in terms of the root mean square errors (RMSE). RMSE values were obtained between 0.02-0.06 for NRTL and UNIQUAC, respectively. For DNN, the error values were obtained between 0.00005-0.01 for all temperatures. According to the calculated RMSE values, it was shown that proposed DNN structure can be better choice for the modelling of LLE system. Othmer-Tobias and Hand correlations were also used for the experimental tie-lines. Distribution coefficient and separation factors were calculated from the experimental data.

1. Introduction

Butyric acid is one of the best known carboxylic acid widely used in chemical and food industries. It is found in animal fat or vegetable oil and can be produced by using whole cell transformation or can be obtained from carbohydrate and renewable resources. Raw material cost and other production costs comprise the most of the production expenditure. Therefore, developing an effective recovery process using alternative recovery methods i.e., adsorption, electrodialysis, solvent extraction etc. is important in producing from bio-based raw materials. In chemical and food industry, when compared to the other separation methods, solvent extraction method is much more preferable due to its low cost. Also, solvent extraction is the prominent extraction method because most of the polar solvents can dissolve acids alone. Consequently, it is used for obtaining pure chemical substances like organometalics in many chemical industries like pharmaceutical or biomedical industries [1–5]. Appropriate solvent selection and determining optimum operation conditions are important for solvent extraction. For this reason, water + butyric acid + 5-methyl-2-hexanone (5M2H, methyl isoamyl ketone) LLE data were determined at 298.2 K, 308.2 K and 318.2 K and P = 101.3 kPa. The solubility curves and the tie-lines were plotted and shown as the ternary phase diagrams for each system. Separation factors (S) and distribution coefficients (D_i) were defined from the tie-line data values to establish the extraction ability of the solvent. The Othmer-Tobias [6] and Hand [7] correlations were used to test the reliability.

Deep neural network (DNN) have been used in many engineering fields such as digital mechanics, earth science, digital physics, life sciences and chemistry. In the field of chemistry, it is used for modeling problems that are very difficult to solve and cannot be solved analytically in subjects such as quantum chemistry and molecular dynamics [8]. The first wave of application of DNN in pharmaceutical research and computational chemistry has emerged in recent years. DNN models have been used successfully in the pharmaceutical industry, especially in the fields of drug design and drug discovery [9–14]. In studies in the field of chemical engineering, a DNN was trained by Zhang et al. as a productive model to guide the relationship between CO_2 adsorption of porous carbons and the corresponding textural properties. The trained DNN was also used to estimate the CO_2 adsorption capacity of unknown porous carbons [15]. Again, in the field of chemical en-

* Corresponding author.
E-mail address: aozmen@khas.edu.tr (A. Özmen).

https://doi.org/10.1016/j.fluid.2021.113094
0378-3812/

Nomenclature

A_{ij}	NRTL binary interaction parameter ($A_{ij} = \Delta g_{ij}/R$)
A, B	Othmer-Tobias equation constants
A', B'	Hand equation constants
b	Bias value
B_{ij}	UNIQUAC binary interaction parameter ($B_{ij} = \Delta u_{ij}/R$)
D_i	Distribution coefficient of component i
Δg_{ij}	NRTL binary parameter for the interaction energy between components i and j relative to the interaction energy of j with itself
g_{ij}	NRTL energy parameter ($Jmol^{-1}$)
N	Number of the tie-lines
$P(x)$	Penalty function
q_i	Relative van der Waals surface area parameter
R	Universal gas constant
R^2	Correlation factor for Othmer-Tobias and Hand equations
$RMSE$	Root mean square error
r	Penalty coefficient
r_i	Relative van der Waals volume parameter
S	Separation factor
T	Temperature (K)
Δu_{ij}	UNIQUAC binary parameter for the interaction energy between components i and j relative to the interaction energy of j with itself
u_{ij}	UNIQUAC energy parameter ($Jmol^{-1}$)
w_{ij}	Weight of input node j on node i
x_i	Mole fraction of component i
x_{ij}	Mole fraction of component i in phase j
x_{ijk}	Experimental mole fraction of component i in phase j along tie-line k
Y_i	Output value of the neuron i
Greek Letters	
α_{ij}	Nonrandomness parameter for component i and j
γ_i	Activity coefficient of component i
γ_{ij}	Activity coefficient of component i in phase j
$\Phi(x)$	Updated objective function
Subscripts	
calc	Calculated values
exp	Experimental values
I	Aqueous phase
II	Solvent phase

gineering, there is a master's thesis study in which DNN approach is used for the simultaneous estimation of density, viscosity and heat capacity of ionic liquids [16]. In another study, a DNN model was presented by Haghighatlari et al. to accurately and effectively predict the refractive index of organic molecules and this was applied to a library of 1.5 million compounds [17]. Apart from these studies, modeling of extraction process and liquid-liquid equilibrium data with DNN is a fairly new study topic in the literature and in chemical engineering.

In this study, liquid-liquid equilibrium (LLE) data of (water + butyric acid + 5M2H) ternaries defined at three different temperatures of 298.2, 308.2, and 318.2 K and P = 101.3 kPa, were obtained experimentally and then correlated with nonrandom two-liquid model (NRTL) and universal quasi-chemical (UNIQUAC) models [18,19]. For the thermodynamic models, the binary interaction parameters were calculated and listed. Deep neural network (DNN) was used to model the system and performance of the proposed DNN model was compared with that of NRTL and UNIQUAC in terms of the root mean square errors (RMSE). Also, new tie-line data were calculated by the proposed DNN model and results were shown in the ternary diagrams to form the solubility curves for all temperatures.

2. Materials and methods

2.1. Chemicals

The chemicals of analytical grade were purchased from Merck. The purity of the chemical reagents was checked by gas chromatography (GC) and was used without further purification. Structural formulas of chemicals and their features were shown in the Table 1 [20]. Distilled water was prepared in our laboratory.

2.2. Experimental procedures

LLE data of (water + butyric acid + 5M2H) ternaries defined at three different temperatures of 298.2, 308.2, and 318.2 K and P = 101.3 kPa were obtained experimentally. Solubility curves and mutual solubility were determined by using the 'Cloud Point' method [21,22]. The cloud point was determined by observing the transition from a homogeneous to a heterogeneous mixture as indicated by the mixture turbidity (cloudiness) [23]. For this purpose, a special glass cell that was connected to the circulating water bath kept at constant temperature. Circulating water bath (NUVE BS302 model) was equipped with a temperature controller capable of maintaining the temperature within ±0.1 K. The cell, designed to contain a solution from (50 to 200) cm^3, was filled with homogeneous (butyric acid + water) mixtures prepared by mass. An electronic Sartorius analytical balance with an accuracy of ±0.0001 g was used. The solvent was progressively added by means of the TITRONIC universal titrator (accurate to 0.01 ml). The end point was determined by observing the transition from a homogeneous to a heterogenous mixture. This pattern was convenient for providing the water-rich side of the curves. The data for the solvent-rich side of the curves were therefore obtained by titrating the homogeneous (butyric acid + solvent) with water until turbidity appeared. All mass fractions were determined and pointed in ternary phase diagrams. Therefore, miscible and immiscible area were determined in diagrams for T = 298.2, 308.2, and 318.2 K. Then on the diagrams, several arbitrary points were chosen in the immiscible area that shows mid-point for tie-lines. For all mid-points, mixtures were prepared and placed onto the thermostated shaker (NUVE ST 30) for 90 min. Preliminary tests showed that these 90 min durations were enough to achieve equilibrium. After shaking, all mixtures were centrifuged for 5 min with 3000 rpm to separate water-rich phase and solvent-rich phase. At the end of the centrifugate period, samples were taken from both phases and analysed. Phases were transferred with special syringes to the separate sample tubes. The liquid samples were analyzed by a Gas Chromatograph (HP6890 model), equipped with thermal conductivity detector (TCD) and flame ionization detector (FID). To obtain quantitative results, the internal standard method was applied. Ethanol was used as an internal standard. Ultra1 (Methyl Siloxane column, 50m x 320μm x 0.17μm) was utilized to distinguish butyric acid and water of samples. FID and TCD detector temperatures were kept at T = 493.2 K while injection port temperature was held at T = 473.2 K. Injections were performed on the split 70/1 mode. Helium was used as a carrier at a rate of 1.2 cm^3 min^{-1}. Oven program was programmed starting from 333.2 K hold for 2 min. The temperature was increased at a rate of 30 K/min and held for 2 min. And finally, the temperature was ramped for 15 K/min and held at this temperature for 10 min. Organic compounds were analyzed by FID and water content was de-

Table 1
Molecular Formula, Source, CAS Registry Number, Mass Fraction Purity and Purity Analysis Method of the Chemicals.

Components	Molecular formula	Source	CAS no.	Mass fraction purity[a]	Purity analysis method[b]
butyric acid	$CH_3(CH_2)_2COOH$	Merck	107-92-6	> 0.99	GC
5-methyl-2-hexanone	$CH_3CO(CH_2)_2CH(CH_3)_2$	Merck	110-12-3	> 0.98	GC
water	H_2O	Distilled, lab. made	7732-18-5		GC

[a] Purities were provided by the manufacturers; the chemicals were used without any additional treatment.
[b] Gas chromatography.

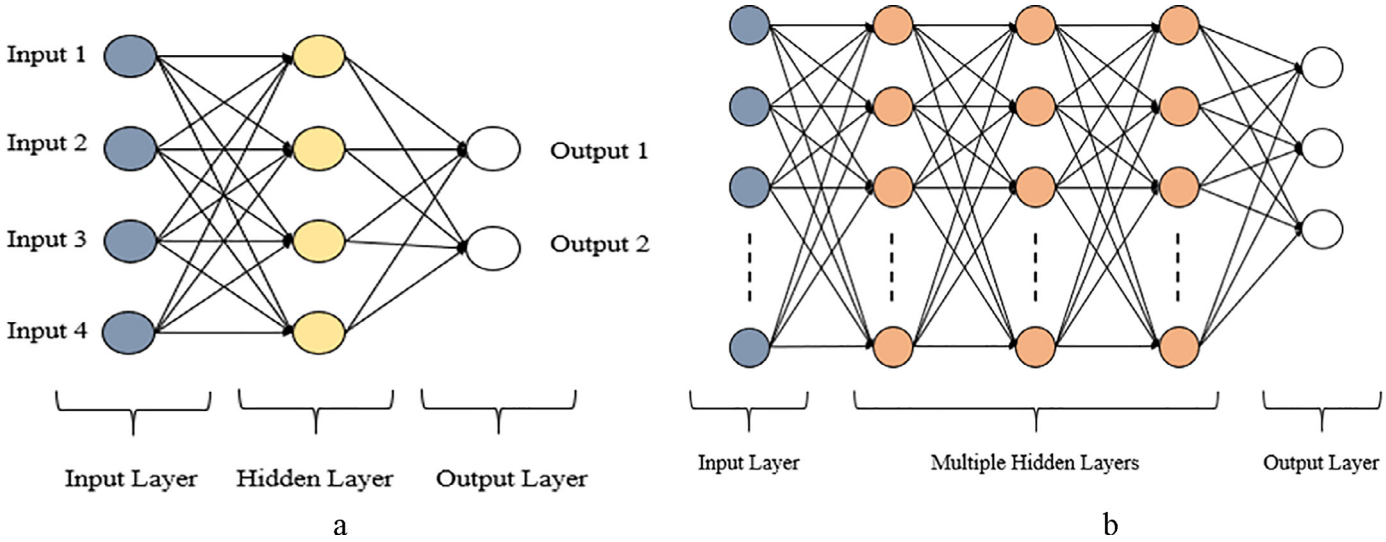

Fig. 1. (a) A simple schematic representation of a traditional ANN with input, hidden and output layers (b) DNN differ from ANN by having multiple hidden layers as depicted in the schematic diagram.

termined using TCD detectors. The uncertainty of the compositions of the tie-lines were within 5×10^{-4} mole fraction.

2.3. Deep neural network

DNN is a subfield of machine learning related to algorithms inspired by the structure and function of the brain called artificial neural networks (ANN) [8]. DNN simulates the human brain's abilities such as observing, analyzing, learning and making decisions for complex problems, and can perform operations such as feature extraction, transformation and classification, with or without supervision, by using large amounts of data [24,25].

Although DNN seems to be a recent past issue, its foundations were laid in the 1940s with artificial intelligence. The first mathematical neural network (NN) was devised by McCulloch and Pitts in an attempt to model a biological neuron [26]. After this great breakthrough, Alan Turing, an English mathematician in 1950, said that machine learning was possible. In 1965, Alexey Ivakhnenko mathematically modeled the first computer-based multi-parameter data sets and applied them to NN. This work laid the foundation of modern DNN used today [8]. In the 2000s, the strengthening of GPU and CPU hardware accelerated the development of DNN. These developments have led to a renaissance in ANN [9,10].

One way to understand DNN models is to compare them with ANN. A comparison of the structure of an ANN and DNN is given in Fig. 1 [27]. The main difference between them is the scale and complexity of the neural network [10]. A typical structure of an ANN and a neuron of a hidden layer unit are represented in Fig. 1a. ANN usually has three layers: an input layer, a hidden layer and an output layer [27]. Nodes (also called neurons) or units in each layer are connected to nodes in adjacent layers. Each link has a weight value. The inputs are multiplied by the respective weights and added up in each unit. The sum then undergoes a transformation based on the activation function; this is, in most cases, a

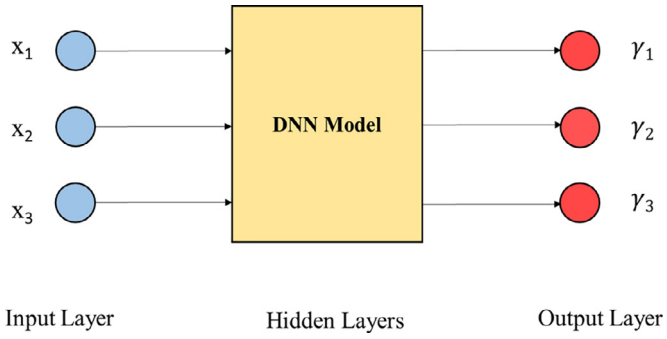

Fig. 2. Schematic diagram of the proposed model.

sigmoid function, a hyperbolic tangent function. The output value Y_i of the neuron i is calculated as shown in Eq. (1). The output of the function is then fed as input to the unit in the next layer. The result of the first output layer is used to solve the problem [10,25].

Finding the correct weights is called training the neural network. Training of the NN is performed by iterative modification of the weight values in the network so as to optimize the error between the actual value and the predicted values [10].

$$Y_i = f\left(\sum_j x_j w_{ij} + b\right) \quad (1)$$

where x_j refers to the input variables, w_{ij} is the weight of input node j on node i, b is bias value and function f is the activation function to transform the linear combination of input signal from input nodes to an output value. The training of an ANN is done by iterative modification of the weight values in the network to optimize the errors between predicted and true value typically through the back-propagation methods [10]. Unlike the ANN, DNN models use more than one non-linear hidden layers for feature extraction

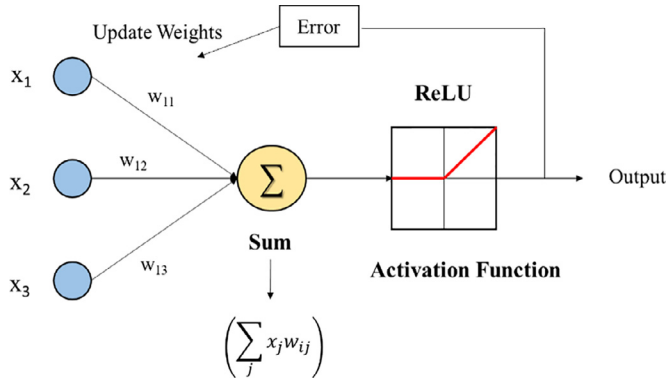

Fig. 3. Neuron model.

and transformation, and each layer can have different functions [8,10,15,27].

2.4. The NRTL and UNIQUAC models

To represent liquid-liquid equilibrium systems, generalized thermodynamic models that relate excess Gibbs energy to the composition of liquids have been proposed by various researchers. These models, described as activity coefficient models, show the dependence of composition and temperature on the activity coefficient. Once the activity coefficients are obtained, the compositions of the species in the equilibrium phases can also be calculated. The NRTL (nonrandom two-liquid) and UNIQUAC (universal quasi-chemical) thermodynamic models are the most widely used activity coefficient models in the literature [28,29]. The NRTL and UNIQUAC models [18,19] were applied to correlate the experimental tie-line data. The activity coefficient for any component i in a multicomponent system is given by the following equation for the NRTL model:

$$\ln \gamma_i = \frac{\sum_{j=1}^{C} \tau_{ji} G_{ji} x_j}{\sum_{k=1}^{C} G_{ki} x_k} + \sum_{j=1}^{C} \left[\frac{x_j G_{ij}}{\sum_{k=1}^{C} G_{kj} x_k} \left(\tau_{ij} - \frac{\sum_{k=1}^{C} x_k \tau_{kj} G_{kj}}{\sum_{k=1}^{C} G_{kj} x_k} \right) \right] \tag{2}$$

where,

$$G_{ij} = \exp(-\alpha_{ij} \tau_{ij}) \tag{3}$$

$$\tau_{ij} = \frac{g_{ij} - g_{jj}}{RT} \qquad \tau_{ji} = \frac{g_{ji} - g_{ii}}{RT} \tag{4}$$

C is the number of the components in the mixture and x_j is the mole fraction of component j. R is the universal gas constant and T is the absolute temperature. g_{ij} and g_{ji} ($g_{ij} = g_{ji}$) are NRTL interaction energies between species i and j. τ_{ij}, τ_{ji} and α_{ij} are the adjustable NRTL model parameters for the binary pair $i - j$. α_{ij} is the nonrandomness parameter of the NRTL equation and usually varies from about 0.2 to 0.47 ($\alpha_{ij} = \alpha_{ji}$). τ_{ij} and τ_{ji} ($\tau_{ij} \neq \tau_{ji}$) are the energy parameters between type i and type j molecules. The UNIQUAC model equation is shown as:

$$\ln \gamma_i = \ln (\Psi_i / x_i) + (\overline{Z}/2) q_i \ln (\theta_i / \Psi_i) + l_i - (\Psi_i / x_i) \sum_{j=1}^{C} x_j l_j + q_i \left[1 - \ln \left(\sum_{j=1}^{C} \theta_j \tau_{ji} \right) - \sum_{j=1}^{C} \left(\frac{\theta_j \tau ij}{\sum_{k=1}^{C} \theta_k \tau_{kj}} \right) \right] \tag{5}$$

where,

$$\Psi_i = \frac{x_i r_i}{\sum_{i=1}^{C} x_i r_i} \tag{6}$$

$$\theta_i = \frac{x_i q_i}{\sum_{i=1}^{C} x_i q_i} \tag{7}$$

$$l_i = \left(\frac{\overline{Z}}{2} \right) (r_i - q_i) - (r_i - 1) \tag{8}$$

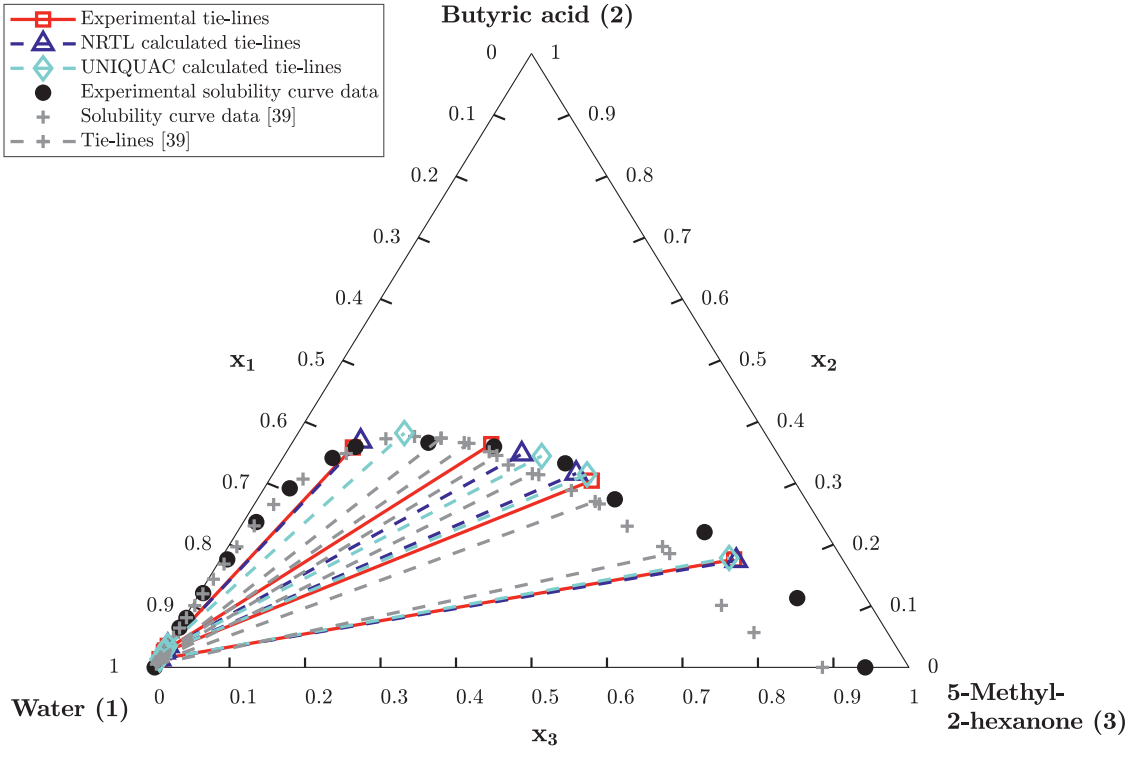

Fig. 4. NRTL, UNIQUAC and experimental phase diagram of LLE data at T = 298.2 K and P = 101.3 kPa.

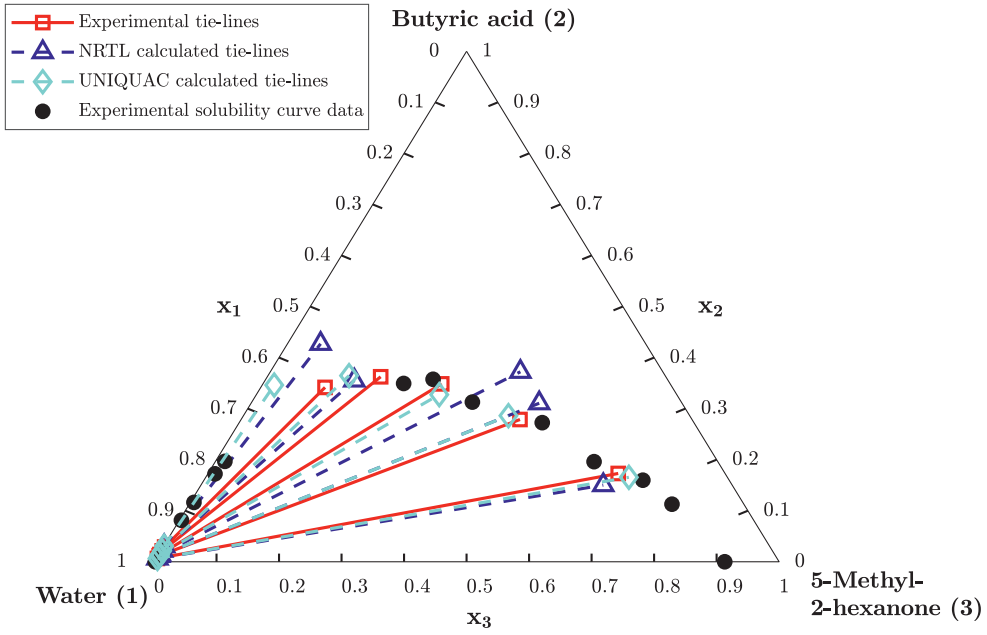

Fig. 5. NRTL, UNIQUAC and experimental phase diagram of LLE data at T = 308.2 K and P = 101.3 kPa.

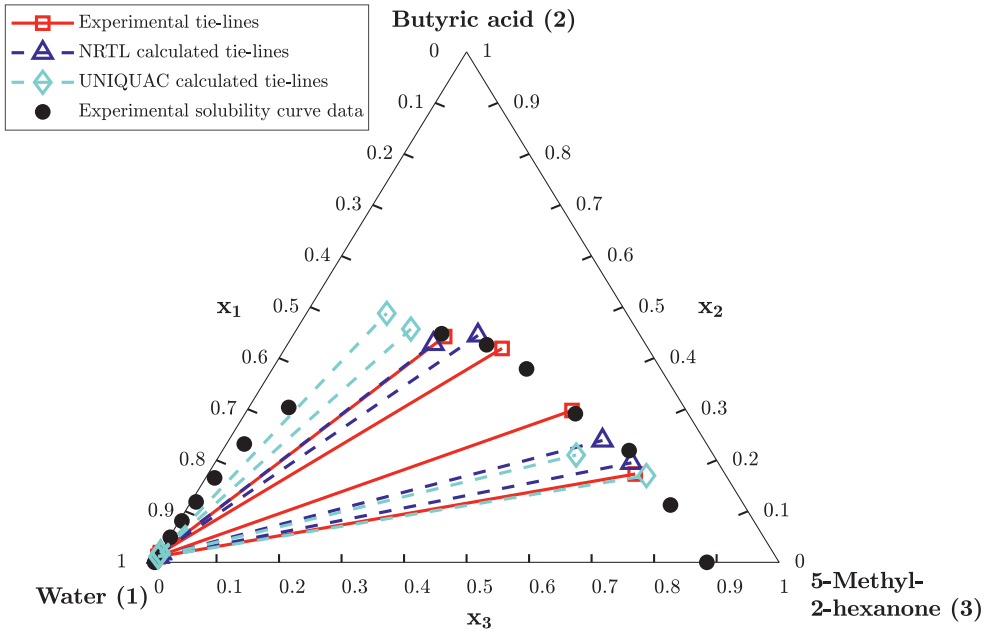

Fig. 6. NRTL, UNIQUAC and experimental phase diagram of LLE data at T = 318.2 K and P = 101.3 kPa.

$$\tau_{ij} = \exp\left(\frac{-\left(u_{ij} - u_{jj}\right)}{RT}\right) \tau_{ji} = \exp\left(\frac{-\left(u_{ji} - u_{ii}\right)}{RT}\right) \tag{9}$$

In these equations, u_{ji} and u_{ij} are the UNIQUAC interaction energies between species i and j ($u_{ij} = u_{ji}$). τ_{ij} and τ_{ji} ($\tau_{ij} \neq \tau_{ji}$) are the energy parameters between type i and type j molecules. Ψ_i and θ_i are the volume and area fraction for species i. $\overline{Z}$ is the lattice coordination number and generally it is set to the value 10. r_i and q_i are volume and surface area parameters for the pure components and calculated from the following equations:

$$r_i = \sum_k \nu_k^{(i)} R_k \tag{10}$$

$$q_i = \sum_k \nu_k^{(i)} Q_k \tag{11}$$

R_k (group-volume) and Q_k (group-area) values are determined for each functional group and are available in the literature [19]. $\nu_k^{(i)}$ denotes the number of functional groups of type k in i.

2.5. Proposed DNN model

In this study, a DNN structure was proposed for the estimation of activity coefficient models of ternary liquid-liquid equilibrium systems. This DNN consists of three inputs, two hidden layers with three neurons in each and three outputs, as shown in Fig. 2. The experimental datas (x_1, x_2 and x_3) were applied to this proposed

Table 2
Experimental Solubility Curve Data for Water (1) + Butyric acid (2) + 5-Methyl-2-Hexanone (3) Ternary Systems at T = (298.2, 308.2, and 318.2) K and P = 101.3 kPa[a].

298.2 K		308.2 K		318.2 K	
x_1	x_2	x_1	x_2	x_1	x_2
0.0579[b]	0.0000	0.0428[b]	0.0000	0.1156[b]	0.0000
0.0916	0.1128	0.0837	0.1128	0.1176	0.1123
0.1606	0.2203	0.1381	0.1598	0.1305	0.2189
0.2527	0.2738	0.1980	0.1961	0.1804	0.2911
0.2891	0.3324	0.2427	0.2725	0.2146	0.3789
0.3698	0.3596	0.3343	0.3128	0.2548	0.4262
0.4536	0.3659	0.3748	0.3575	0.3160	0.4478
0.5534	0.3592	0.4260	0.3493	0.6328	0.3034
0.5930	0.3411	0.7883	0.1967	0.7397	0.2318
0.6744	0.2917	0.8163	0.1723	0.8204	0.1654
0.7462	0.2367	0.8780	0.1163	0.8735	0.1183
0.8151	0.1759	0.9155	0.0813	0.9149	0.0810
0.8745	0.1210	0.9755	0.0221	0.9494	0.0491
0.9168	0.0806	0.9978[b]	0.0000	0.9778	0.0211
0.9339	0.0647			0.9990[b]	0.0000
0.9707	0.0284				
0.9992[b]	0.0000				

[a] Standard uncertainties u are u(x) = 0.003. u(T) = 0.2 K and u(P) = 0.7 kPA.
[b] Mutual solubility value.

DNN structure as input and activity coefficients (γ_1, γ_2 and γ_3) were selected as output data. Bias values are assumed to be zero.

The training process that takes place in the perceptron is shown in the Fig. 3. Mathematical model of neuron called perceptron is a fundamental unit of a NN [30]. The ReLU function introduced by ref [31] was used as the activation function in the proposed DNN structure. It has been shown that the ReLU function, which has a strong biological and mathematical basis, improves the training of DNN and provides a significant performance increase in DNN compared to other activation functions. Therefore, it is the most used activation function in DNN today [32]. ReLU function works by thresholding values at 0, i.e., $f(x) = max(0, x)$. Simply put, it gives a linear function if $x \geq 0$, and equals 0 when $x < 0$. So, any negative value is returned as zero by the ReLU function (Fig. 3).

At the first step, γ values that satisfies LLE conditions shown in Eq. (12) were obtained.

$$x_i^I \gamma_i^I = x_i^{II} \gamma_i^{II}, i = 1, 2, 3 \tag{12}$$

where, i is the component index. I and II show water-rich and solvent-rich phases, respectively.

To obtain non-zero activity coefficients satisfying Eq. (12), the following objective function is minimized and corresponding DNN weights were obtained for the given experimental data.

$$F_1 = \sum_{j=1}^{N} \sum_{i=1}^{3} \frac{(x_{ij}^I \gamma_{ij}^I - x_{ij}^{II} \gamma_{ij}^{II})^2}{(x_{ij}^I \gamma_{ij}^I + x_{ij}^{II} \gamma_{ij}^{II})^2} \tag{13}$$

where x_{ij}^I and x_{ij}^{II} refer to the experimental mole fraction of component i of water-rich and solvent-rich phase, respectively, along tie-line j, γ_{ij}^I, and γ_{ij}^{II} are the corresponding activity coefficients and N shows the number of the tie lines.

Two steps hybrid optimization method was used to calculate DNN, NRTL and UNIQUAC model parameters. First, the simulated annealing (SA) algorithm which is a probability-based heuristic algorithm inspired by the fact that the atoms of the solids gradually cool down, was applied and then Nelder-Mead simplex search algorithm [33] was used for the optimization of the weights [34,35]. After the achieving the equilibrium condition, the activity coefficient values are obtained using the proposed DNN model.

After minimizing the first objective function, the obtained coefficients were used for testing. At the test step, DNN weight coefficients that are obtained by minimizing F_1 were used to correlate experimental tie lines. For this purpose, only mole fraction of water obtained from the water-rich phase x_{1k}^I, are given to the proposed DNN system and then the mole fractions x_{2k}^I, x_{1k}^{II} and x_{2k}^{II} were determined by minimizing the following objective function,

$$F_2 = \sum_{i=1}^{3} \frac{(x_{ik}^I \gamma_{ik}^I - x_{ik}^{II} \gamma_{ik}^{II})^2}{(x_{ik}^I \gamma_{ik}^I + x_{ik}^{II} \gamma_{ik}^{II})^2}, \quad k = 1, 2, ..., N \tag{14}$$

with constraints, $0 < x_{2k}^I < 1$, $0 < x_{1k}^{II} < 1$, $0 < x_{2k}^{II} < 1$ and $x_{1k}^{II} + x_{2k}^{II} < 1$. Where subscript k represents kth tie line.

The penalty function method is used for our constrained optimization problem [36–38]. The constraint function that is shown in Eq. (14) is converted to an unconstrained optimization problem by introducing some penalty terms. The general expression of the unconstrained function is as follows:

$$\Phi(\mathbf{x}) = F_2(\mathbf{x}) + rP(\mathbf{x}) \tag{15}$$

where, r and $P(\mathbf{x})$ show scalar optimization constant and penalty function, respectively. The penalty coefficient r was selected as 100.

Table 3
Experimental, NRTL Model and UNIQUAC Model Calculated Tie-Line Data for Water (1) + Butyric acid (2) + 5-Methyl-2-Hexanone (3) Ternary Systems at T = (298.2. 308.2. and 318.2) K and P = 101.3 kPa with RMSE values[a].

NRTL Model								UNIQUAC Model							
Water-rich phase				Solvent-rich phase				Water-rich phase				Solvent-rich phase			
x_{11}		x_{21}		x_{13}		x_{23}		x_{11}		x_{21}		x_{13}		x_{23}	
Exp.	Model	Exp.	Model	Exp.	Model	Exp.	Model	Exp.	Model	Exp.	Model	Exp.	Model	Exp.	Model
$T = 298.2K$; $RMSE = 0.0146$								$T = 298.2K$; $RMSE = 0.0288$							
0.9860	0.9860	0.0134	0.0134	0.1436	0.1418	0.1759	0.1738	0.9860	0.9860	0.0134	0.0134	0.1436	0.1491	0.1759	0.1782
0.9746	0.9746	0.0247	0.0247	0.2681	0.2829	0.3042	0.3159	0.9746	0.9746	0.0247	0.0247	0.2681	0.2692	0.3042	0.3144
0.9718	0.9718	0.0275	0.0275	0.3715	0.3392	0.3636	0.3474	0.9718	0.9718	0.0275	0.0275	0.3715	0.3143	0.3636	0.3443
0.9643	0.9643	0.0350	0.0350	0.5575	0.5421	0.3582	0.3683	0.9643	0.9643	0.0350	0.0349	0.5575	0.4776	0.3582	0.3816
$T = 308.2K$; $RMSE = 0.0419$								$T = 308.2K$; $RMSE = 0.0261$							
0.9913	0.9913	0.0065	0.0064	0.1709	0.2062	0.1730	0.1502	0.9913	0.9913	0.0065	0.0064	0.1709	0.1576	0.1730	0.1655
0.9859	0.9859	0.0118	0.0116	0.2752	0.2285	0.2787	0.3106	0.9859	0.9859	0.0118	0.0118	0.2752	0.2899	0.2787	0.2862
0.9835	0.9835	0.0142	0.0140	0.3655	0.2278	0.3485	0.3722	0.9835	0.9835	0.0142	0.0142	0.3655	0.3800	0.3485	0.3274
0.9762	0.9762	0.0214	0.0217	0.4562	0.5020	0.3624	0.3552	0.9762	0.9762	0.0214	0.0215	0.4562	0.5057	0.3624	0.3646
0.9685	0.9685	0.0290	0.0304	0.5556	0.5200	0.3416	0.4270	0.9685	0.9685	0.0290	0.0306	0.5556	0.6346	0.3416	0.3462
$T = 318.2K$; $RMSE = 0.0255$								$T = 318.2K$; $RMSE = 0.0567$							
0.9882	0.9882	0.0109	0.0109	0.1437	0.1388	0.1730	0.1949	0.9882	0.9882	0.0109	0.0108	0.1437	0.1273	0.1730	0.1699
0.9871	0.9871	0.0120	0.0120	0.1826	0.1632	0.2974	0.2387	0.9871	0.9871	0.0120	0.0119	0.1826	0.2196	0.2974	0.2102
0.9812	0.9812	0.0177	0.0177	0.2337	0.2595	0.4190	0.4445	0.9812	0.9812	0.0177	0.0179	0.2337	0.3606	0.4190	0.4570
0.9798	0.9798	0.0191	0.0191	0.3139	0.3391	0.4423	0.4278	0.9798	0.9798	0.0191	0.0194	0.3139	0.3838	0.4423	0.4877

[a] Standard uncertainties u are u(x) = 0.0005, u(T) = 0.2 K and u(P) = 0.7 kPA.

Table 4
Experimental and DNN Model Calculated Tie-Line Data for Water (1) + Butyric acid (2) + 5-Methyl-2-Hexanone (3) Ternary Systems at T = (298.2. 308.2. and 318.2) K and P = 101.3 kPa with RMSE values[a].

Water-rich phase				Solvent-rich phase			
x_{11}		x_{21}		x_{13}		x_{23}	
Exp.	Model	Exp.	Model	Exp.	Model	Exp.	Model
$T = 298.2K$; $RMSE = 0.0026$							
0.9860	0.9860	0.0134	0.0134	0.1436	0.1436	0.1759	0.1758
0.9746	0.9746	0.0247	0.0247	0.2681	0.2673	0.3042	0.2974
0.9718	0.9718	0.0275	0.0275	0.3715	0.3657	0.3636	0.3640
0.9643	0.9643	0.0350	0.0350	0.5575	0.5578	0.3582	0.3577
$T = 308.2K$; $RMSE = 0.0122$							
0.9913	0.9913	0.0065	0.0065	0.1709	0.1709	0.1730	0.1731
0.9859	0.9859	0.0118	0.0120	0.2752	0.2970	0.2787	0.3062
0.9835	0.9835	0.0142	0.0143	0.3655	0.3510	0.3485	0.3411
0.9762	0.9762	0.0214	0.0213	0.4562	0.4600	0.3624	0.3590
0.9685	0.9685	0.0290	0.0293	0.5556	0.5544	0.3416	0.3453
$T = 318.2K$; $RMSE = 0.00005$							
0.9882	0.9882	0.0109	0.0109	0.1437	0.1437	0.1730	0.1730
0.9871	0.9871	0.0120	0.0120	0.1826	0.1826	0.2974	0.2974
0.9812	0.9812	0.0177	0.0177	0.2337	0.2336	0.4190	0.4189
0.9798	0.9798	0.0191	0.0191	0.3139	0.3139	0.4423	0.4423

[a] Standard uncertainties u are u(x) = 0.0005, u(T) = 0.2 K and u(P) = 0.7 kPA.

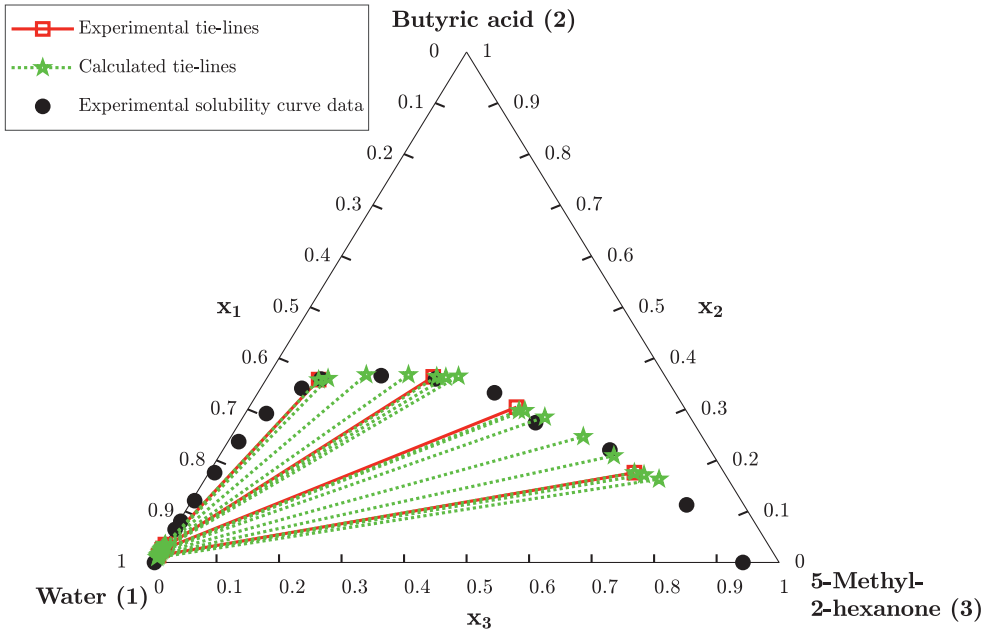

Fig. 7. DNN and experimental phase diagram of LLE data at T = 298.2 K and P = 101.3 kPa.

According to the constraints of the Eq. (14), the penalty function was defined the sum of the quadratic loss functions as shown in Eq. (16).

$$P(\mathbf{x}) = \sum_{j=1}^{m} max[0, p_j(\mathbf{x})]^2$$
$$p_1 = x_{2k}^{I} - 1$$
$$p_2 = x_{1k}^{II} - 1$$
$$p_3 = x_{2k}^{II} - 1$$
$$p_4 = -x_{2k}^{I}$$
$$p_5 = -x_{1k}^{II}$$
$$p_6 = -x_{2k}^{II}$$
$$p_7 = x_{1k}^{II} + x_{2k}^{II} - 1 \quad (16)$$

The objective functions shown in Eqs. (13) and (14) were also used for the optimization of the NRTL and UNIQUAC model parameters. After the optimization process, errors between experimental and all models were calculated using Root Mean Square Error (RMSE) that is given as follows:

$$RMSE = \sqrt{\frac{\sum_{k=1}^{N}\sum_{j=1}^{3}\sum_{i=1}^{3}(x_{ijk}^{exp.} - x_{ijk}^{calc.})^2}{6N}} \quad (17)$$

2.6. Tie-lines, distribution coefficients and separation factor

To test the consistency of the experimental tie- lines, the Othmer-Tobias [6] (Eq. (18)) and Hand [7] (Eq. (19)) correlations were used.

$$\ln\left(\frac{1-x_{33}}{x_{33}}\right) = A + B\ln\left(\frac{1-x_{11}}{x_{11}}\right) \quad (18)$$

$$\ln\left(\frac{x_{23}}{x_{33}}\right) = A' + B'\ln\left(\frac{x_{21}}{x_{11}}\right) \quad (19)$$

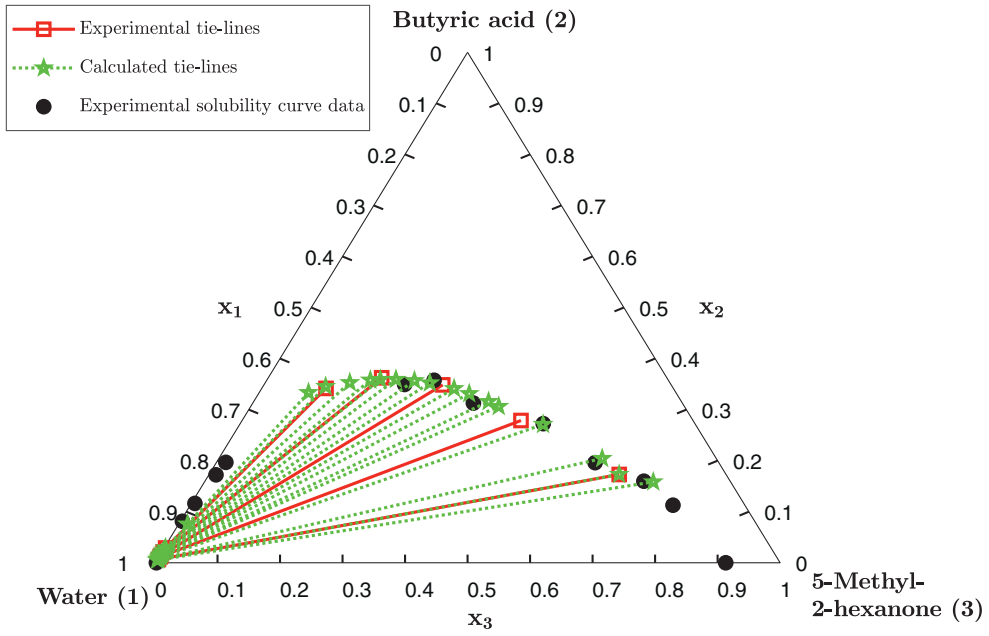

Fig. 8. DNN and experimental phase diagram of LLE data at T = 308.2 K and P = 101.3 kPa.

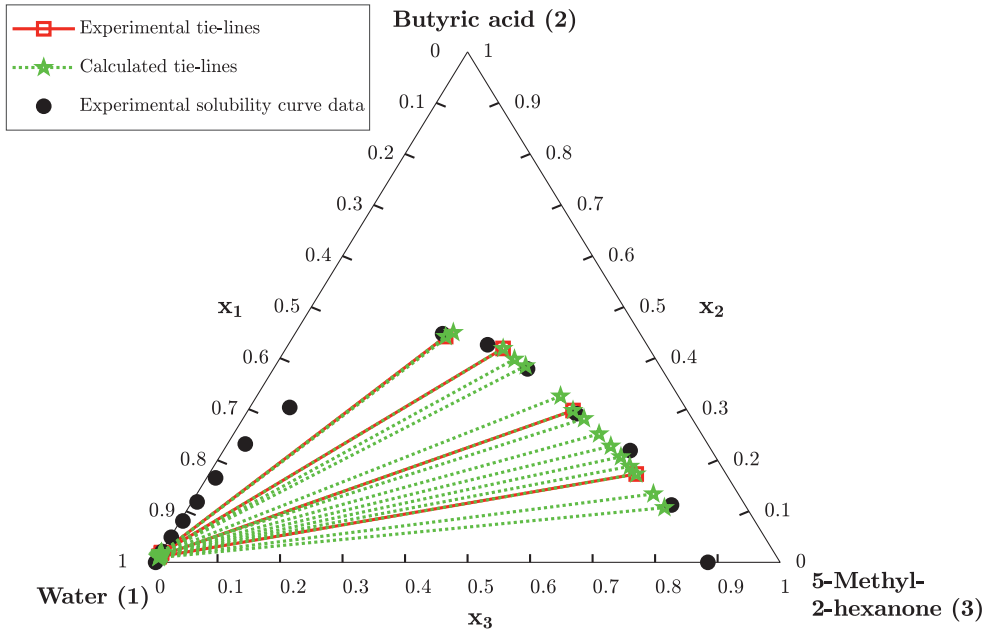

Fig. 9. DNN and experimental phase diagram of LLE data at T = 318.2 K and P = 101.3 kPa.

where x_{11} is mole fraction of water in water-rich phase; x_{21} and x_{23} are mole fractions of the butyric acid in water-rich and solvent-rich phases, respectively; x_{33} is mole fraction of the solvent in solvent-rich phase.The slope of the lines gives the parameters B and B', and the constants give the parameters A and A'. The correlation coefficients and correlation factor (R^2) values were determined by the least-squares method. The linearity of the lines and the correlation factors being approximately to 1 indicates the degree of consistency of the related data.

In order to evaluate the efficiency of 5M2H in the recovery of butyric acid from its aqueous solutions, distribution coefficients (D_i) for water ($i = 1$) and butyric acid ($i = 2$) and separation factor (S) were calculated using the following equations:

$$D_i = \frac{x_{i3}}{x_{i1}} \tag{20}$$

$$S = \frac{D_2}{D_1} \tag{21}$$

Distribution coefficient of acid provided the extraction capacity of solvent which was the first criteria in choosing an extraction process. The higher distribution coefficient value means less solvent needed in extraction.

3. Results and discussions

The experimental solubility curves data of ternary systems (water + butyric acid + 5M2H) at T = 298.2, 308.2, and 318.2 K at P = 101.3 kPa are respectively tabulated in Table 2. 5M2H has been used as a solvent by other researchers in the literature [39–41]. The experimental tie-line and calculated NRTL [18] and UNI-

Table 5
DNN Model Calculated Tie-Line Data for Water (1) + Butyric acid (2) + 5-Methyl-2-Hexanone (3) Ternary Systems at T = (298.2. 308.2. and 318.2) K and P = 101.3 kPa.

Water-rich phase			Solvent-rich phase		
x_{11}	x_{21}	x_{31}	x_{13}	x_{23}	x_{33}
$T = 298.2K$					
0.9900	0.0096	0.0004	0.1104	0.1633	0.7263
0.9875	0.0121	0.0004	0.1302	0.1718	0.6980
0.9840	0.0155	0.0005	0.1598	0.2091	0.6311
0.9810	0.0185	0.0005	0.1899	0.2466	0.5635
0.9775	0.0219	0.0006	0.2324	0.2848	0.4828
0.9755	0.0238	0.0007	0.2580	0.2977	0.4443
0.9740	0.0254	0.0006	0.3303	0.3651	0.3046
0.9725	0.0268	0.0007	0.3517	0.3628	0.2855
0.9700	0.0292	0.0008	0.4090	0.3678	0.2232
0.9675	0.0317	0.0008	0.4765	0.3677	0.1558
0.9650	0.0343	0.0007	0.5413	0.3605	0.0982
$T = 308.2K$					
0.9940	0.0053	0.0007	0.1237	0.1584	0.7179
0.9915	0.0069	0.0016	0.1825	0.2043	0.6132
0.9890	0.0094	0.0016	0.2437	0.2710	0.4853
0.9855	0.0124	0.0021	0.3085	0.3158	0.3757
0.9845	0.0134	0.0021	0.3317	0.3313	0.3370
0.9815	0.0162	0.0023	0.3842	0.3523	0.2635
0.9800	0.0176	0.0024	0.4066	0.3567	0.2367
0.9780	0.0195	0.0025	0.4350	0.3592	0.2058
0.9750	0.0225	0.0025	0.4766	0.3578	0.1656
0.9725	0.0251	0.0024	0.5120	0.3528	0.1352
0.9100	0.0758	0.0142	0.5877	0.3334	0.0789
$T = 318.2K$					
0.9900	0.0091	0.0009	0.1315	0.1071	0.7614
0.9890	0.0101	0.0009	0.1357	0.1340	0.7303
0.9865	0.0125	0.0010	0.1465	0.1880	0.6655
0.9855	0.0134	0.0011	0.1513	0.2067	0.6420
0.9845	0.0144	0.0011	0.1570	0.2276	0.6154
0.9835	0.0153	0.0012	0.1638	0.2516	0.5846
0.9825	0.0163	0.0012	0.1730	0.2814	0.5456
0.9815	0.0173	0.0012	0.1884	0.3257	0.4859
0.9810	0.0178	0.0012	0.2146	0.3849	0.4005
0.9806	0.0182	0.0012	0.2260	0.3979	0.3761
0.9805	0.0185	0.0010	0.2977	0.4501	0.2522

Table 6
NRTL and UNIQUAC Binary Interaction Parameters for the Water (1) + Butyric acid (2) + 5-Methyl-2-Hexanone (3) Ternary Systems at T = (298.2, 308.2 and 318.2) K.

		NRTL model (α_{ij}[a])	UNIQUAC model
	i, j[b]	$A_{ij} = (g_{ij} - g_{jj})/R$	$B_{ij} = (u_{ij} - u_{jj})/R$
$T = 298.2K$	1,2	1520.484	233.148
	2,1	−477.973	−52.850
	1,3	1962.615	159.660
	3,1	404.255	503.586
	2,3	437.040	45.946
	3,2	−157.203	34.913
$T = 308.2K$	1,2	1033.091	405.039
	2,1	1701.439	53.879
	1,3	1676.420	293.226
	3,1	770.519	663.875
	2,3	−228.910	112.848
	3,2	666.328	−26.641
$T = 318.2K$	1,2	1061.730	−262.027
	2,1	1410.060	13902.592
	1,3	2167.379	−183.900
	3,1	942.490	717.348
	2,3	13.602	−6.882
	3,2	623.421	210.087

[a] $\alpha_{ij} = 0.2$ for $T = 298.2K$, $\alpha_{ij} = 0.37$ for $T = 308.2K$ and $T = 318.2K$.
[b] i-j pair of components: water (1), butyric acid (2), 5-methyl-2-hexanone (3).

Table 7
The Volume (r_i) and Surface Area (q_i) Structural Parameters for the UNIQUAC Model.

Component	r	q
Water	0.920	1.400
Butyric acid	3.551	3.152
5-Methyl-2-Hexanone	5.270	4.492

Table 8
Fitting Parameters in Hand and Othmer-Tobias Equations for the Water + Butyric acid + 5-Methyl-2-Hexanone Ternary Systems (R^2: regression coefficient).

Temperature	Hand correlation			Othmer-Tobias correlation		
	A'	B'	R^2	A	B	R^2
T=298.2 K	9.9346	2.6700	0.9033	11.9770	3.0522	0.8829
T=308.2 K	7.1548	1.6877	0.9840	9.6088	2.1721	0.9872
T=318.2 K	12.0180	2.9172	0.9285	12.5370	2.9664	0.9382

Table 9
Experimental Values of the Distribution Coefficients (D_i) for the Water (1) and Butyric acid (2) and the Separation Factors (S) at T=298.2 K, T=308.2 K, T=318.2 K and P = 101.3 kPa.

	D_1	D_2	S
T=298.2 K	0.15	13	90
	0.28	12	45
	0.38	13	35
	0.58	10	18
T=308.2 K	0.17	27	155
	0.28	24	85
	0.37	25	66
	0.47	17	36
	0.57	12	21
T=318.2 K	0.15	16	110
	0.18	25	134
	0.24	24	99
	0.32	23	72

QUAC [19] models data of the studied systems were reported in Table 3 and Figs. 4–6, in which x_{i1} and x_{i3} refer to mole fractions of the ith component in the water-rich and solvent-rich phase, respectively. Fig. 4 also shows tie-lines and solubility curve data taken from [39]. The DNN and experimental data results were presented in Table 4. The RMSE values for NRTL, UNIQUAC and DNN models, were also given in Tables 3-4. From Tables 3-4, when compared with NRTL and UNIQUAC, it can be seen that, the minimum RMSE values are obtained using the proposed DNN model. For NRTL and UNIQUAC, while RMSE values were obtained between 0.0146 and 0.0567, for DNN, these values were between 0.00005 and 0.0122. The calculated tie-line data were obtained for various water mole fraction values and results are presented in Table 5. For different temperature values, calculated and experimental tie-lines with solubility curve data are given in Figs. 7–9. From the figures, it can be said that, the solubility curve data and tie-line data agree well with the calculated data obtained from the proposed DNN method. In LLE calculation, it is important to use true equilibrium compositions that satisfy the isoactivity condition. A global stability test like the Gibbs-Duhem equation can be used to guarantee the stability of the solution. The thermodynamics consistency of our proposed DNN model data is tested using Gibbs-Duhem equations. However, the Gibbs-Duhem equation could not be achieved and we think this is due to numerical derivative calculation errors.

The optimized NRTL and UNIQUAC binary interaction parameters of the researched ternary systems are reported in Table 6. The volume (r_i) and area (q_i) structural parameters for the UNIQUAC model are given in Table 7. The Othmer-Tobias and Hand correlations are shown in Figs. 10 and 11. The correlation coeffi-

Table 10
Comparison of Separation Factors (Highest Values) for the (Water + Butyric Acid + Solvent) ternary Systems at different temperatures and P = 101.3 kPa.

Ternary System	Solvent Type	S	T, K	Reference Number
water + BA + 5M2H	ketone	90	298.2	This study
water + BA + 5M2H	ketone	155	308.2	This study
water + BA + 5M2H	ketone	134	318.2	This study
water + BA + methyl isoamyl ketone	ketone	154.6	298.2	[39]
water + BA + butanal	aldehyde	88.05	293.15	[42]
water + BA + butanal	aldehyde	100.16	308.15	[42]
water + BA + butanal	aldehyde	97.89	323.15	[42]
water + BA + isoamyl acetate	ester	133.7	298.2	[39]
water + BA + dimethyl maleate	ester	13.03	298.2	[43]
water + BA + 1-heptanol	alcohol	106.8	298.2	[44]
water + BA + 1-heptanol	alcohol	96.8	308.2	[44]
water + BA + 1-heptanol	alcohol	95.3	318.2	[44]
water + BA + decanol	alcohol	208	298.2	[45]
water + BA + decanol	alcohol	173	308.2	[45]
water + BA + decanol	alcohol	135	318.2	[45]
water + BA + n-butanol	alcohol	39.47	293.15	[42]
water + BA + n-butanol	alcohol	36.48	308.15	[42]
water + BA + n-butanol	alcohol	30.03	323.15	[42]
water + BA + undecanol	alcohol	85.20	298.2	[46]

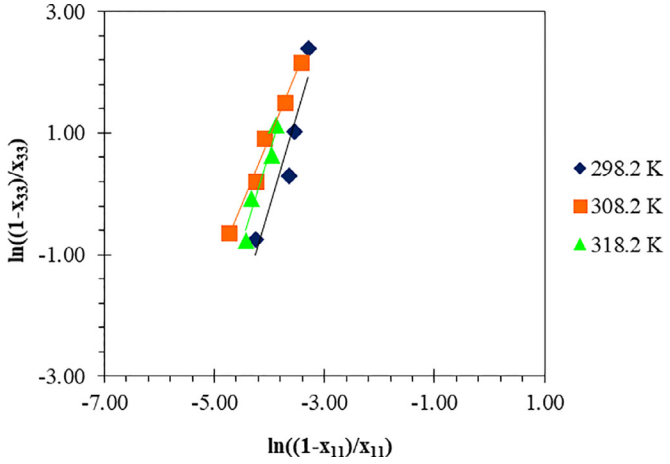

Fig. 10. Othmer-Tobias plot for LLE data of the water + butyric acid + 5-methyl-2-hexanone ternary systems at T = (298.2, 308.2, and 318.2) K and P = 101.3 kPa.

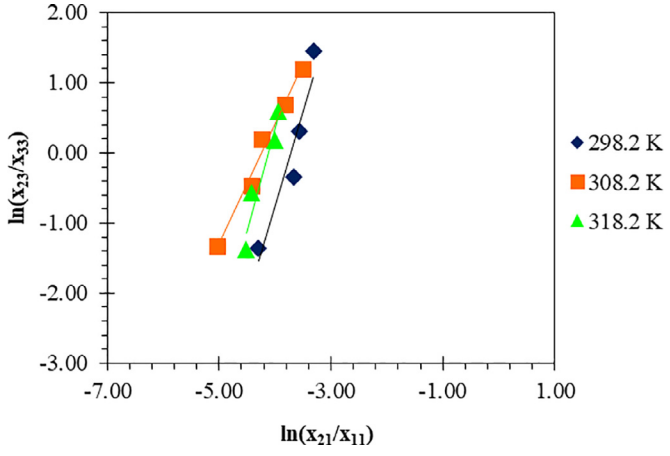

Fig. 11. Hand plot for LLE data of the water + butyric acid + 5-methyl-2-hexanone ternary systems at T = (298.2, 308.2, and 318.2) K and P = 101.3 kPa.

cients and correlation factor (R^2) values are given in Table 8. The separation factors and distribution coefficients for the ternary systems were presented in Table 9. For similar ternary aqueous systems, the comparison of the highest values of the separation factors obtained in this study and previously reported in the literature [39,42–46] are given in Table 10 and Fig. 12. As can be seen, extracting capabilities of the solvents not only depend on the solvent type but also depend on the temperature. The highest and lowest separation factor values was obtained for decanol [45], and dimethyl maleate [43], respectively at 298 K. In this study, in addition to propose a new model, we also examined the effect of temperature on equilibrium data by performing precise temperature control. The separation factors were calculated as 90, 155 and 134 at 298.2 K, 308.2 K, and 318.2 K, respectively. The separation factor value given by the researchers who have examined the same system in the literature [39] for 298.2 K is closer to the result we found for 308.2 K. Figs. 13 and 14 show the distribution coefficients of butyric acid (D_2) and separation factors (S) as a function of the mole fraction of butyric acid in water-rich phase (x_{21}) for 5M2H at T = 298.2, 308.2, and 318.2 K, respectively.

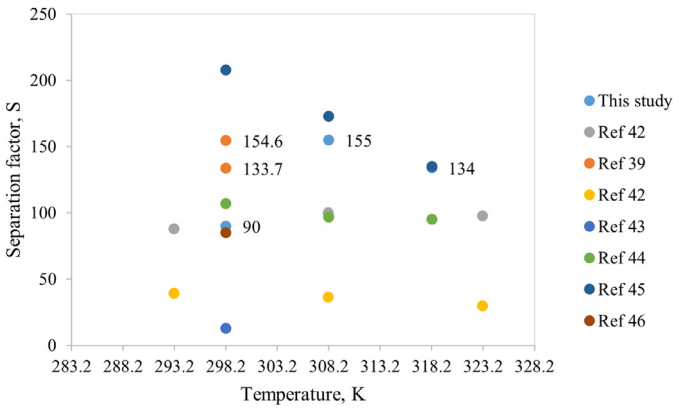

Fig. 12. Comparison of Separation Factors (Highest Values) for the (Water + Butyric Acid + Solvent) ternary systems at different temperatures and P = 101.3 kPa.

4. Conclusions

In this study, modelling of LLE data are considered using NRTL, UNIQUAC and DNN model. Experimental LLE data of the ternary systems (water + butyric acid + 5M2H) were measured at T = 298.2, 308.2, and 318.2 K temperatures and at P = 101.3 kPa. No data on these ternary systems at 308.2 K and 318.2 K have been found in the literature. Performance of the proposed DNN model is

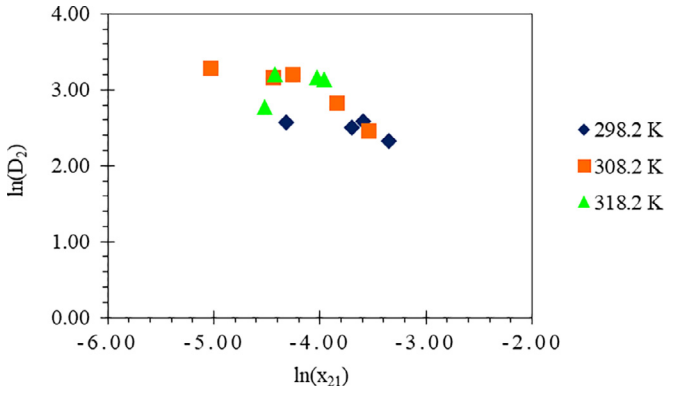

Fig. 13. Distribution coefficients of butyric acid (D_2) as a function of the mole fraction of butyric acid in water-rich phase (x_{21}) for water (1) + butyric acid (2) + 5-methyl-2-hexanone (3) ternary systems at T = (298.2, 308.2, and 318.2) K and P = 101.3 kPa.

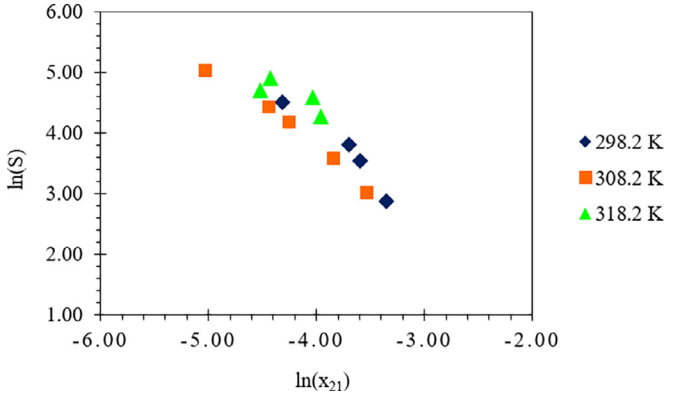

Fig. 14. Separation factors (S) as a function of the mole fraction of butyric acid in water-rich phase (x_{21}) for water (1) + butyric acid (2) + 5-methyl-2-hexanone (3) ternary systems at T = (298.2, 308.2, and 318.2) K and P = 101.3 kPa.

compared to well known NRTL and UNIQUAC models by means of RMSE. From the calculated RMSE values, when compared to NRTL and UNIQUAC models, it was shown that the proposed model gives much lower RMSE values. Since the activity coefficient models have a non-linear structure, the ReLU activation function is used for all layers to introduce this nonlinearity to the proposed DNN model. Also the number of the parameters used in DNN is much more than that of NRTL and UNIQUAC. Therefore it can be said that the proposed DNN model outperforms to UNIQUAC and NRTL models. Also the experimental results were successfully correlated with the Othmer-Tobias and Hand correlation methods. Distribution coefficients (D) and the separation factors (S) values do not change with temperature. Based on the D and S, it can be said that 5M2H is suitable for the extraction of butyric acid from aqueuos solution.

Declaration of Competing Interest

The authors declare that they have no known competing financial interests or personal relationships that could have appeared to influence the work reported in this paper.

CRediT authorship contribution statement

Sezin Bekri: Writing - original draft, Data curation, Visualization, Formal analysis. **Dilek Özmen:** Writing - review & editing, Supervision, Validation. **Aykut Türkmenoğlu:** Resources, Investigation. **Atilla Özmen:** Conceptualization, Methodology, Software.

Acknowledgements

This work was supported by Scientific Research Projects Coordination Unit of Istanbul University. Project Numbers: FYL-2016-3732 and YADOP/10662

References

[1] R.E. Treybal, Mass-Transfer Operations, 3rd ed., Mcgraw-Hill Inc., Singapore, 1981.
[2] J.D. Holbrey, R.D. Rogers, Green Chemistry and Ionic Liquids: Synergies and Ironies, Industrial Applications for Green Chemistry, American Chemical Society, Washington, 2002.
[3] J. Rydberg, M. Cox, C. Musikas, G.R. Choppin, Solvent Extraction Principles and Practice, second ed., Marcel Dekker, Inc., New York, 2004.
[4] A. Şenol, Optimum extraction equilibria of the systems (water + carboxylic acid + 1-hexanol/alamine): thermodynamic modeling, Fluid Phase Equilib. 360 (2013) 77–87.
[5] C.S. López-Garzón, A.J.J. Straathof, Recovery of carboxylic acids produced by fermentation, Biotechnol. Adv. 32 (2014) 873–904.
[6] D.F. Othmer, P.E. Tobias, Liquid-liquid extraction data-toluene and acetaldehyde systems, J. Ind. Eng. Chem. 36 (1942) 690–692.
[7] D.B. Hand, Dineric distribution, J. Phys. Chem. 34 (1930) 1961–2000.
[8] Y.A. Ayturan, Forecasting of particulate matter concentration with deep learning method, KTO Karatay University The Graduate School of Natural and Applied Sciences, 2019 Master's thesis.
[9] A. Şeker, B. Diri, H.H. Balık, A review about deep learning methods and applications, Gazi Mühendislik Bilimleri Dergisi 3 (3) (2017) 47–64.
[10] H. Chen, O. Engkvist, Y. Wang, M. Olivecrona, T. Blaschke, The rise of deep learning in drug discovery, Drug Discov. Today 23 (6) (2018) 1241–1250.
[11] M. Shin, D. Jang, H. Nam, K.H. Lee, D. Lee, Predicting the absorption potential of chemical compounds through a deep learning approach, IEEE/ACM Trans. Comput. Biol. Bioinform. 15 (2) (2018) 432–440.
[12] G.B. Goh, N.O. Hodas, A. Vishnu, Deep learning for computational chemistry, J. Comput. Chem. 38 (2017) 1291–1307.
[13] S.R. Johnson, W. Zheng, Recent progress in the computational prediction of aqueous solubility and absorption, AAPS J. 8 (1) (2006) E27–40.
[14] S. Kwon, S. Yoon, Deep CCI: end-to-end deep learning for chemical-chemical interaction prediction, ACM-BCB'17, 2017.
[15] Z. Zhang, J.A. Schott, M. Liu, H. Chen, X. Lu, B.G. Sumpter, J. Fu, S. Dai, Prediction of carbon dioxide adsorption via deep learning, Angew. Chem. 131 (2019) 265–269.
[16] K. Sakloth, Simultaneous prediction of density, viscosity and heat capacity of ionic liquids-a deep learning approach, University of Washington, 2018 Master's thesis.
[17] M. Haghighatlari, G. Vishwakarma, M.A.F. Afzal, J. Hachmann, A physics-infused deep learning model for the prediction of refractive indices and its use for the large-scale screening of organic compound space, ChemRxiv (2019), doi:10.26434/chemrxiv.8796950.v1.
[18] H. Renon, J.M. Prausnitz, Local compositions in thermodynamic excess functions for liquid mixtures, AIChE J. 14 (1968) 135–144.
[19] B.E. Poling, J.M. Prausnitz, J.P. O'Connell, The Properties of Gases and Liquids, 50th ed., McGraw-Hill Inc.,, New York, 2001.
[20] D.R. Lide, CRC Handbook of Chemistry and Physics, 89th ed., (Internet Version), CRC Press, Boca Raton, Florida, 2009.
[21] L. Alders, Liquid-Liquid Extraction, second ed., Elsevier, Amsterdam, 1959.
[22] A. Şenol, S. Cehreli, D. Özmen, Phase equilibria for the ternary liquid systems of (water + tetrahydrofurfuryl alcohol + cyclic solvent) at 298.2 K, J. Chem. Eng. Data 50 (2005) 688–691.
[23] A. Merzougui, A. Hasseine, A. Kabouche, M. Korichi, LLE for the extraction of alcohol from aqueous solutions with diethyl ether and dichloromethane at 293.15 K, parameter estimation using a hybrid genetic based approach, Fluid Phase Equilib. 309 (2011) 161–167.
[24] K. Kayaalp, A.A. Süzen, Derin Öğrenme ve Türkiyedeki Uygulamaları, IKSAD Publishing House, 2018.
[25] A. Shrestha, A. Mahmood, Review of deep learning algorithms and architectures, IEEE Access 7 (2019) 53040–53065.
[26] W. McCulloch, W. Pitts, A logical calculus of ideas immanent in nervous activity, Bull. Math. Biophys 5 (1943) 115–133.
[27] C. Fan, F. Xiao, Y. Zhao, A short-term building cooling load prediction method using deep learning algorithms, Appl. Energy 195 (2017) 222–233.
[28] H. Renon, J.M. Prausnitz, Estimation of parameters for the NRTL equation for excess Gibbs energies of strongly nonideal liquid mixtures, I&EC Process Des. Dev. 8 (3) (1969) 413–419.
[29] J.D. Seader, E.J. Henley, D.K. Roper, Separation Process Principles: Chemical and Biochemical Operations, third ed., John Wiley & Sons, Inc., USA, 2011.
[30] A. Gupta, Introduction to deep learning: Part 1, CEP AIChE J. (2018) 22–29.
[31] R.H.R. Hahnloser, R. Sarpeshkar, M.A. Mahowald, R.J. Douglas, H.S. Seung, Digital selection and analogue amplification coexist in a cortex-inspired silicon circuit, Nature 405 (2000) 947–951.
[32] A.F.M. Agarap, Deep learning using rectified linear units (ReLU), arxiv (2019).
[33] J. Lagarias, J. Reeds, M. Wright, P. Wright, Convergence properties of the Nelder-Mead simplex method in low dimensions, SIAM J. Optim. 9 (1) (1998) 112–147.

[34] S. Kirkpatrick, C.D. Gelatt, M.P. Vechi, Optimization by simulated annealing, Science 220 (1983) 671–680.
[35] Y. Avcı, Damage detection of mechanical systems in finite element model updating method using simulated annealing algorithm, İstanbul Technical University, Institute of Science and Technology, 2008 Master's thesis.
[36] C.A. Coello Coello, Theoretical and numerical constraint-handling techniques used with evolutionary algorithms: a survey of the state of the art, Comput. Methods Appl. Mech. Eng. 191 (2002) 1245–1287.
[37] B. Tessema, G.G. Yen, A self adaptive penalty function based algorithm for constrained optimization, in: in Proc. Evol. Comput. CEC IEEE Congr. IEEE, 2006, pp. 246–253.
[38] O. Yeniay, Penalty function methods for constrained optimization with genetic algorithms, Math. Comput. Appl. 10 (1) (2005) 45–56.
[39] H.G. Gilani, A.G. Gilani, S.L.S. Saadat, Experimental and correlational study of phase equilibria in aqueous solutions of formic and butyric acids with isoamyl acetate and methyl isoamyl ketone at T = 298.15 K, J. Chem. Eng. Data 59 (2014) 917–925.
[40] D. Özmen, (Liquid + liquid) equilibria of (water + propionic acid + methyl isoamyl ketone or diisobutyl ketone or ethyl isoamyl keton) at T = 298.2 K, Fluid Phase Equilib. 250 (2006) 70–75.
[41] H. Ghanadzadeh Gilani, A. Ghanadzadeh Gilani, S. Shekarsaraee, Experimental study of phase equilibria in aqueous mixtures of phosphoric acid with isoamyl acetate and methyl isoamyl ketone at T = (298.2, 308.2, and 318.2) K, Fluid Phase Equilib. 337 (2013) 32–38.
[42] C. Yu, S. Wu, Y. Zhao, Z. Zeng, W. Xue, Liquid–liquid equilibrium data of water + butyric acid + Butanal or n-Butanol ternary systems at 293.15, 308.15, and 323.15 K, J. Chem. Eng. Data 62 (2017) 2244–2252.
[43] D. Özmen, Determination and correlation of liquid-liquid equilibria for the (water + carboxylic acid + dimethyl maleate) ternary systems at T = 298.2 K, Fluid Phase Equilib. 269 (2008) 12–18.
[44] A. Ghanadzadeh Gilani, H. Ghanadzadeh Gilani, S.L.S. Saadat, E. Nasiri-Touli, M. Peer, Liquid-liquid equilibrium data in aqueous solutions of propionic and butyric acids with 1-heptanol at T=(298.15, 308.15, and 318.15) K, Korean J. Chem. Eng. 33 (4) (2016) 1408–1415.
[45] S.I. Kirbaslar, Liquid-liquid equilibria of the water + butyric acid + decanol ternary system, Braz. J. Chem. Eng. 23 (2006) 365–374.
[46] T. Gündoğdu, S. Cehreli, Ternary liquid-liquid phase equilibria of (water-carboxylic acid-1-undecanol) systems at 298.15 K, Fluid Phase Equilib. 331 (2012) 26–32.